Journal of Applied Fluid Mechanics, Vol. 11, No. 3, pp. 733-742, 2018.
Available online at www.jafmonline.net, ISSN 1735-3572, EISSN 1735-3645.
DOI: 10.29252/jafm.11.03.28506

Effect of Boost Pressure on the In-Cylinder Tumble-Motion of GDI Engine under Steady-State Conditions using Stereoscopic-PIV

Mohammed El Adawy[1†], M. R. Heikal[1, 2], A. Rashid A. Aziz[1], S. Munir[1, 3] and M. I. Siddiqui[1, 4]

[1]*Mechanical Engineering Department, University Technology PETRONAS, Perak, Seri Iskandar, 32610, Centre for Automotive Research and Electric Mobility (CAREM),*
[2]*University of Brighton, Brighton BN2 4GJ, UK*
[3]*Department of Mathematics, COMSATS Institute of Information Technology, park road, chak shehzadcampus, tarlai kalan, 44000 Islamabad, Pakistan*
[4]*Nust Institute of Civil Engineering (NICE), National University of Science and Technology (NUST), 44000 Islamabad, Pakistan*

†*Corresponding Author Email: engmohammed_2008@yahoo.com*

(Received October 9, 2017; accepted December 23, 2017)

ABSTRACT

This paper experimentally investigates the effect of boost pressure on the in-cylinder flow field under steady-state conditions using stereoscopic particle image velocimetry (Stereo-PIV) through increasing the pressure difference across the intake valves. The FEV steady-state flow bench was modified to provide an optical access into the cylinder region. The stereoscopic PIV measurements were carried out at various pressure differences viz., 300, 450, and 600 mmH_2O across the intake valves of Gasoline Direct Injection (GDI) head for the mid cylinder vertical tumble-plane. Ensemble average velocity vectors were used to characterize the tumble flow structure and for the calculation of tumble ratio and average turbulent kinetic energy. Moreover, the Proper Orthogonal Decomposition (POD) technique was conducted on the PIV measured velocity vector maps to identify the most energetic structures generated at different valve lifts and pressure differences. The results of stereoscopic PIV measurements showed that the overall in-cylinder flow structures were mainly dependent on the valve lift irrespective of the applied pressure difference. However, the level of the turbulence kinetic energy increased as the boost pressure increased.

Keywords: In-cylinder flow; Tumble motion; Boosted GDI engine; Stereo PIV- POD.

NOMENCLATURE

GDI	Gasoline Direct Injection
PFI	Port Fuel Injection
POD	Proper Orthogonal Decomposition
PIV	Particle Image Velocimetry
TKE	Turbulent Kinetic Energy
TR	Tumble Ratio
TSI	Turbo-Stratified Injection
VL	Valve Lift

1. INTRODUCTION

Driven by increasingly stringent emission regulations and better fuel economy, the automotive industry turned towards downsized boosted gasoline direct injection engines as the most powerful enabler to meet these requirements. As a matter of fact, this concept is intended to expand high load and low engine speed regions against natural aspirated engines by utilizing turbocharger, supercharger or in more advanced designs turbo-stratified injection (TSI) which lead to an improvement of the fuel economy Ricardo *et al.* (2011). GDI engines provide significant merits compared with multi-point port fuel injection (PFI) systems. These advantages include reducing the throttling losses, higher thermal efficiency, higher compression ratios, lower fuel consumption, lower CO2 and HC emissions and higher volumetric efficiency Zhao *et al.* (1999), Smith *et al.* (2006). GDI engines can work under two different mixture modes, a homogenous mixture mode is applied at full load while a stratified mixture mode is applied at part loads Preussner *et al.* (1998), Fraidl *et al.* (1996). In stratified mode, three different combustion systems are used to maintain a combustible mixture at the instant of ignition near

the spark plug. These are wall-guided, air-guided and spray-guided. The specific differentiation between theses combustion systems depends on whether the fuel spray impinges on the piston head, the in-cylinder flow or the fuel spray features and dynamics are used to realize the concept of stratification Ortmann *et al*. (2001). The improvement of the first generation of GDI engines has been mainly focused on the wall-guided combustion system, while the second generation of GDI is oriented on the spray-guided system. However, it is important to acknowledge that regardless of this classification, the stratification achievement of real system is accomplished by some combination of these three combustion systems Zhao *et al*. (1999). Basically, the structure of the in-cylinder flow field during the inlet and compression strokes is one of the key factors in the process of mixture preparation in internal combustion engines and particularly in GDI engines. A proper compromise between two aspects is essential during the air-fuel mixing process; a certain level of turbulence is essential in order to enhance the air-fuel mixing, but very high levels of turbulence may affect the stabilization of the stratification process. The admission flow inducted through the intake valves can be divided into two large scale motions; swirl (exploited in compression ignition (CI) engines) and tumble (targeted in spark ignition (SI) engines) Kim *et al*. (2006). These kinds of flow structures are strongly dependent on the profile of the intake port Bari and Saad (2013), Zhang *et al*. (2014), piston shape Brusiani *et al*. (2014), Buhl *et al*. (2017) and valve lift profile Clenci *et al*. (2014), Li *et al*. (2017). The tumble motion offers the advantages of preserving stable mixture stratification, compensating for the slow flame speed and enhancing the idle stability and the EGR susceptibility thus, it is notably important to modern GDI engines Li *et al*. (2001), Wang *et al*. (2015), Fu *et al*. (2016). Moreover, there is a limitation in the achievement of thermal efficiency at high load and low engine speed which is considered as a significant problem in the development of a boosted GDI engine. To solve this issue, many researchers worked on the optimization of the intake port and combustion chamber shape, while others investigated the introduction of a switching device for flow enhancement in the cylinder such as a tumble control valve Adomeit *et al*. (2010). Therefore, it is of significant important to gain a complete understanding of in-cylinder tumble motion characteristics for boosted GDI engines.

Steady flow test benches have been extensively used for assessing the characteristics of in cylinder flow. However, these studies have been limited to integral flow parameters such as tumble ratio, swirl ratio, flow coefficient, and discharge coefficients El-Adawy *et al*. (2017b). With the advent of more sophisticated mixture flow strategies in engines to meet the recent pollution standard, the understanding of in-cylinder flow characteristics became more than ever a challenge for the research community. Therefore, there is a pressing need to gain more detailed information on the flow characteristics such as turbulence structures, turbulent kinetic energy, turbulent intensity…etc., as these parameters have significant effect on air/fuel mixing process.

In the current study, the FEV steady-state flow bench was modified and used for the in-cylinder flow visualization and measurement of full velocity vector fields in the cylinder. One of the key tools that offer valuable understanding of the instantaneous aerodynamic in spark ignition SI engines is particle image velocimetry (PIV). More recently, a new extension is denoted as high speed time-resolved stereoscopic particle image velocimetry (TR-SPIV) which enables the possibility to obtain sequences of temporally and spatially correlated image pairs. That is of most significance to improve the mixture formation and the combustion stability understanding particularly in GDI engines Lee *et al*. (2007).

Recently, proper orthogonal decomposition (POD) has been considered as a promising tool to accurately extract and identify the coherent structures in turbulent flows. POD was first announced to the turbulence research community by Lumley Lumley (1967). POD analysis can be carried out either on experimental or numerical simulation data sets. POD analytical technique has been extensively adopted by many researchers to study engine cycle-to-cycle variations Chen *et al*. (2011), Liu *et al*. (2013), Chen *et al*. (2013), Tumble motion evolution at different valve lifts under steady-state conditions Mohammed El- Adawy *et al*. (2017a), spray and combustion process Graftieaux *et al*. (2001), Bizon *et al*. (2009), Sick *et al*. (2012).

The objective of the research project described here was to study how the in-cylinder flow structures inside a cylinder of GDI engine were formed and how they were influenced by valve lift and pressure difference. Therefore, a steady-state flow bench was adopted to apply stereoscopic PIV measurements for the mid cylinder vertical plane (plane of symmetry) at different valve lifts 2mm, 5mm and 9mm and different pressure differences across the intake valves 300, 450, and 600 mmH_2O. Moreover, POD was conducted on the PIV velocity vector maps to extract the coherent structures impeded inside the in-cylinder flow and to know how the relative level of flow in energy in the different flow structures were distributed.

Finally, it is hoped that the experimental results from this study provide a better understanding of how relying on steady-state measurements allow more detailed knowledge on the flow structures generated in the engine cylinder and consequently reduce the need for the more expensive in-cylinder measurements in optical engines and facilitates a simpler validation of numerical predictions.

2. EXPERIMENTAL SET UP

In this study, a pent-roof, four valves gasoline direct injection engine head was used for conducting the experiments. A transparent cylinder liner was made of Plexiglas with 92.5 mm diameter and 116 mm stroke length and a flat piston placed at the bottom was used to provide an optical access through the full stroke length. The experiments were carried out at

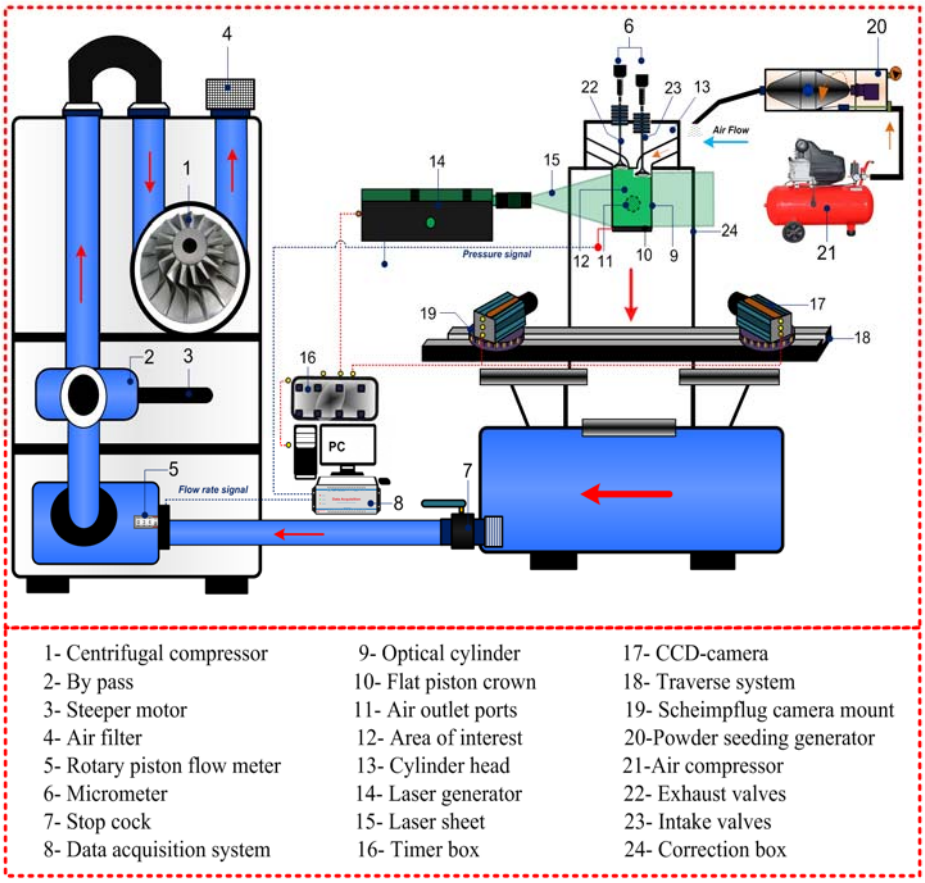

Fig. 1. Schematic for Stereo-PIV set up on steady-state flow bench.

different valve lifts 2mm, 5mm and 9mm and different pressure differences between the cylindrical tube and atmosphere 300, 450, and 600 mmH_2O. The cylinder head was mounted on a steady-state flow bench, which consisted of a centrifugal compressor working under suction conditions. Air was inducted through the intake port, intake valves, the cylindrical tube, the compensation tank and through the rotary piston gas meter then finally discharging to atmosphere. The air flow rate was measured using a rotary piston flow meter which operated on the positive-displacement principle. The deviation of the pressure values was measured using a relative pressure sensor while the pressure adjustment, which was required for different valve lift settings, was achieved by a bypass controlled by stepper motor.

The schematic of the experimental setup for the Stereo-PIV measurements on the modified steady-state flow bench is shown in Fig. 1. A high speed time resolved Stereoscopic PIV system (2D3C, Dantec Dynamics) was used to obtain detailed flow field measurements in the vertical tumble plane (plane of symmetry), as shown in Fig. 2. Titanium Dioxide (TiO_2) solid particles were used as a seeding material and mixed with air at the intake port. A double pulsed Nd: YLF laser capable of 20 mJ at 1 kHz at 527nm per laser head per pulse was used to illuminate the field of view twice with a time interval between pulses adjusted in the range 5 -100 μs depending on the air velocities corresponding to the applied pressure difference. A pair of Speed Sense M310 Dantec Dynamics 12 bit digital output CCD high speed cameras with 1280 pixels by 800 pixels resolution was used in order to capture the particle displacement. Band-pass filters of central wave length of 527 nm were attached to the CCD cameras in order to minimize light reflections. The Scheimpflug principle was fulfilled when the best focus over the entire image, for each camera, was achieved using a special Scheimpflug camera mount. Moreover, the calibration was carried out by means of a standard calibration target which had a well-defined grid of dots. The standard calibration target was one-sided plate containing black dots on a white background spacing of 5 mm and a size of 100 mm by 100 mm. Dynamic Studio V5 software was used for image acquisition and data post-processing. The evaluation was conducted using adaptive correlation techniques with an interrogation area size of 32×32 pixels and 50% overlapping. Ensemble average velocity vectors were computed from the 1000 raw image pairs at the required valve lift and pressure difference.

3. PROPER ORTHOGONAL DECOMPOSITION (POD)

Using the method of snapshot illustrated by Sirovich Sirovich (1987), the POD decomposes a set of

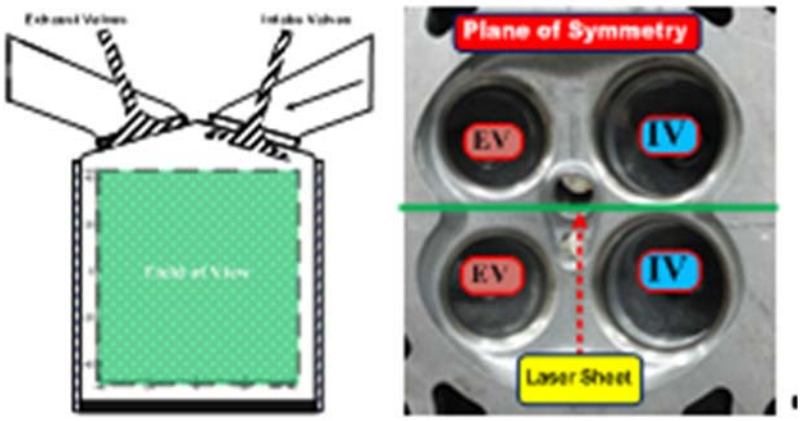

Fig. 2. Mid-cylinder plane (plane of symmetry)

velocity distributions with total number of (**K**) into a linear combination of (**M**) spatial basis functions (or space-dependent POD modes, (denoted $\boldsymbol{\varphi}_m$) and their corresponding time-dependent coefficients, (denoted $\mathbf{C}_m^{(k)}$).

$$(V)^{(k)} = \sum_{m=1}^{M} \mathbf{C}_m^{(k)} \times \boldsymbol{\varphi}_m \qquad (1)$$

The POD code in previous paper Mohammed El-Adawy *et al*. (2017) was employed here. The code mathematically minimizes the following:

$$\sum_{k=1}^{k} \left\| (V)^{(k)} - \sum_{m=1}^{M'} \mathbf{C}_m^{(k)} \times \boldsymbol{\varphi}_m \right\|^2 \rightarrow min \qquad (2)$$

Since $\boldsymbol{\varphi}_m$ are normalized and $\mathbf{C}_m^{(k)}$ is the amplitude, $\frac{1}{2}(\mathbf{C}_m^{(k)})^2$ quantifies the kinetic energy (KE) per unit mass the m_{th} mode contributes in the k_{th} velocity field.

$$KE_m = \frac{1}{2}(\mathbf{C}_m^{(k)})^2 \qquad (3)$$

4. RESULTS AND DISCUSSTIONS

In this section, the results obtained from the PIV and POD analysis are presented. Firstly, the ensemble average velocity vector fields obtained from instantaneous velocity vector fields of 1000 raw images and vorticity contours are shown to give an overview and understanding of the behavior of the in-cylinder flow at different pressure differences across the inlet valves. Moreover, the tumble ratio and the average turbulent kinetic energy were calculated at every valve lift.

4.1 Influence of the Pressure Difference on the flow Structures

Figure 3 depicts the ensemble average velocity vector fields at different pressure differences for different valve lifts. The first observation which can be made is that increasing the pressure difference across the intake valves or the valve lift led to an increase in air flow rate into the cylinder ,as would be expected, and subsequently an increase in air velocities. The maximum velocity approximately correlated well with the Bernoulli calculations for the maximum inlet velocities; for 300 mmH_2O case was (72 m/sec), for 450 mmH_2O case was (90 m/sec), and for 600 mmH_2O case was (102 m/sec). At low valve lift (2 mm), the flow was highly restricted at the area between the valve and valve seat. The restriction was more pronounced on the right side of the intake valves because of the orientation of the intake port which resulted in high pressure drop across the intake valves. Therefore, significant amount of the incoming flow was directed towards the exhaust side because of its inertia and the highly restricted area. Then because of the low pressure area under the intake valves the flow moved from the exhaust side to the intake side and then was deflected by the right cylinder wall and the flat piston surface forming a clock-wise vortex (reverse-tumble).

At mid valve lift (5 mm), the problems associated with the restriction became less and it was clear that there was symmetrical velocity distribution between both jets coming from both sides of the intake valves. These symmetrical distributions led to no-tumble motion at this valve lift. At high valve lift (9 mm), the left hand side air jet was more dominant. Because of the interaction of this jet with the combustion chamber walls and the left cylinder wall then with flat piston, the in-cylinder flow was dominated by a well-defined strong counter-clock-wise vortex (tumble). It was reported that a well-defined tumbling single vortex is more stable than any other large scale in-cylinder flow structures which may break up by the end of compression stroke into small scale structures increasing the level of turbulence during the combustion khalighi (1991). Furthermore, in case of comparing the data for the same valve lift but for different values of pressure difference, the effect of the pressure difference on the flow behavior was negligible compared to the effect of valve lift. This meant that the mean motion was much more dependent on the valve lift than the pressure difference across the intake valves. This was highly required since it ensured the same flow structures for all engine speeds.

4.2 Influence of the Pressure Difference on Vorticity

Vorticity is defined by the curl of the velocity vector. For a three dimensional vector field the vorticity is defined by:

$$curl\ V = \nabla \times V = \left(\frac{\partial v_z}{\partial y} - \frac{\partial v_y}{\partial z}\right) \underset{i}{\rightarrow} + \left(\frac{\partial v_x}{\partial z} - \frac{\partial v_z}{\partial x}\right) \underset{j}{\rightarrow} + \left(\frac{\partial v_y}{\partial z} - \frac{\partial v_{zx}}{\partial y}\right) \underset{k}{\rightarrow} \quad (4)$$

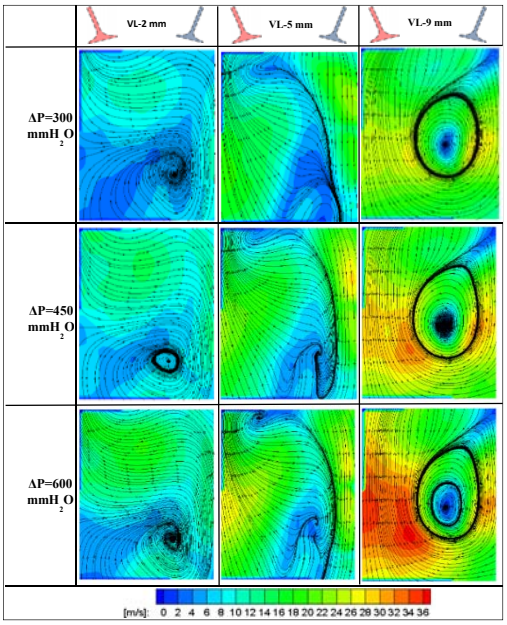

Fig. 3. Ensemble average flow fields at different valve lifts and pressure differences.

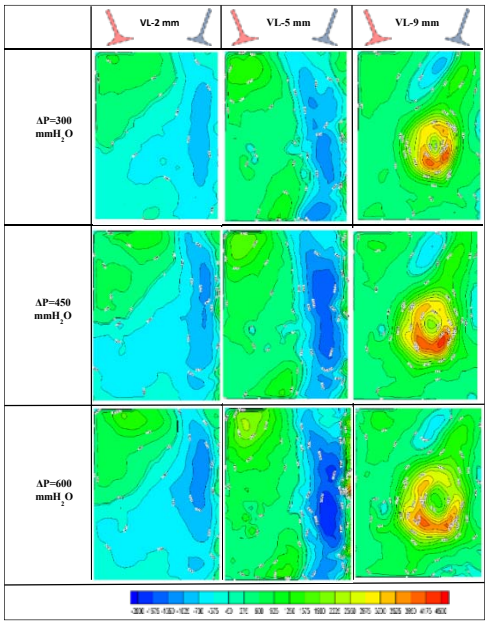

Fig. 4. Vorticity Magnitudes at Different valve lifts and Pressure Differences.

Where V is the velocity vector and $\vec{i}$, $\vec{j}$ and $\vec{k}$ are the unit vectors in x, y and z axis.

Figure 4 shows the variation in the vorticity contours caused by increasing pressure difference for various valve lifts. As can be seen, the formed vortices preserved their shape for the same valve lift for different pressure differences. The only difference in all cases was that the vortex strength increased with increasing the pressure difference. It was also noticed that at 2 mm valve lift, the dominant feature was the reverse tumble motion in the clock wise direction. At 5 mm valve lift, there was a balance between normal tumble and reverse tumble motions. However, at 10 mm valve lift, a strong normal tumble vortex dominated the in-cylinder flow in counter clock wise direction.

4.3 Influence of the Pressure Difference on Tumble Ratio

The tumble ratio (TR) was calculated at different valve lifts from the averaged vorticity obtained from PIV data on the target plane. The mean vorticity was assessed by considering the rotation of the vertical and horizontal velocity components of a particle about the center of the field of view as given Krishna *et al.* (2016):

$$\mathrm{TR} = \frac{\sum_{i=1}^{n}\left(\frac{\partial v}{\partial x} - \frac{\partial u}{\partial y}\right)_i}{2n\omega} \quad (5)$$

where 'n' is total number of grid points, v and u represent velocity components in vertical (y) and horizontal (x) directions respectively and ω is the angular speed of the crank shaft (rad/sec) which was estimated based on constant axial velocity across the bore in the steady port flow bench condition and was defined as Yang *et al.* (2017):

$$\omega = \frac{4\dot{m}}{B^2 S \rho_{cyl}} \quad (6)$$

Where, $\dot{m}$ is the air mass flow rate (kg/sec), S is the engine stroke (m), ρ_{cyl} is the air density (kg/m^3), and B is the cylinder bore (m).

Figure 5 shows the evolution of the tumble ratio at various valve lifts and different pressure differences. It can be seen that the tumble ratio and therefore the mean motion was much more dependent on the valve lift than on the pressure difference. This is highly desirable since it guarantees the same flow structures for all pressure differences and subsequently for all engine speeds. This is consistent with the work of both Krishna Krishna *et al.* (2011) and Zhang Zhang *et al.* (2015). It can be also noticed that at valve lift 2mm, the negative values of tumble ratio were an indication of the reverse tumble motion in the clock-wise direction. However at 5 mm valve lift, the symmetrical velocity distribution led to almost no tumble motion inside the cylinder therefore, the tumble ratio value was almost zero. The positive values of tumble ratio at 9 mm valve lift, were an indication of the strong normal tumble motion in counter clock-wise direction.

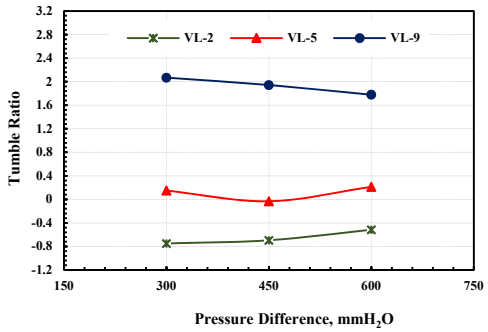

Fig. 5. Evolution of the tumble ratio as a function of the pressure difference and the valve lift.

4.4 Influence of the Pressure Difference on Avg. Turbulent Kinetic Energy

The strength of the turbulence of the in-cylinder air flow is usually related to the so called turbulent kinetic energy (TKE). In the current study, the Avg.TKE of the in-cylinder flow was calculated from the root mean square (RMS) velocity vector fields as follow Reuss (2000):

$$TKE = \frac{1}{2}\,\rho\, V_{rms}^2 = \frac{1}{2}\rho(u_{rms}^2 + v_{rms}^2 + w_{rms}^2) \quad (7)$$

where 'u_{rms}' ,'v_{rms}' and 'w_{rms}' are the RMS velocity components in the x , y and z directions respectively, and 'ρ' is the air density.

Figure 6 shows the variation of the average turbulent kinetic energy with valve lift for different pressure differences. Generally, the Avg.TKE increased with increasing the valve lift and pressure difference as more mass of air entered to the cylinder. However, it was noticed that, the rate of increase was higher from 5 mm to 9 mm valve lift compared to the rate of increase from 2 mm to 5 mm valve lift for all pressure differences.

This might be attributed to the fact that, the increase in intake valve opening led to higher velocity of the air jet entering the cylinder, which had high mean and fluctuating velocity components. It was found also that the Avg.TKE increased by about 36.7 % and 10.7 % for valve lift 9 mm when the pressure difference increased from 300 to 450 mmH_2O, and from 450 to 600 mmH_2O respectively.

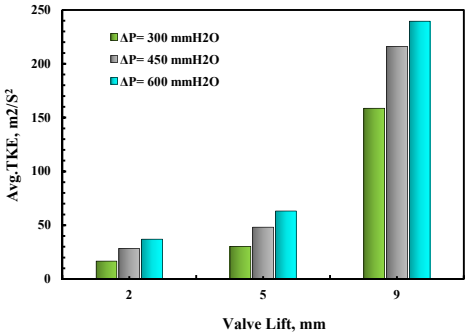

Fig. 6. Avg.TKE at different valve lifts and pressure differences.

4.5 Proper Orthogonal Decomposition (POD)

POD analysis was typically applied on the fluctuating velocity fields after subtracting the ensemble average from each instantaneous velocity field. With a view to study the energy distribution inside the cylinder, the relative energy curves were added at different pressure differences under various valve lifts. Modes 1 and mode 2 structures and their corresponding time dependent coefficients were also presented and discussed below.

4.5.1 Relative Energy Distribution at Different Pressure Differences for Various Valve Lifts

The relative energy distribution curves for different pressure differences at various valve lifts are presented in Fig. 7. It is worth pointing out that, if the flow can be described with a small number of POD modes, this indicates that the structure of the flow in such a situation is relatively simple. Conversely, if the spatial structure of the flow is complex, then the energy will be distributed on a large number of modes and hence a relatively large number of modes is required for an accurate representation of the flow field Fogleman *et al.* (2004).

With these comments in mind, it can be noticed firstly that the relative energy distribution corresponding to the first POD modes for all cases was quite small which gave an indication to the complexity of the flow. Secondly, it can be observed also that there were no significant differences in the relative energy distribution since the flow structure had not changed with changing the pressure differences across the intake valves as discussed earlier.

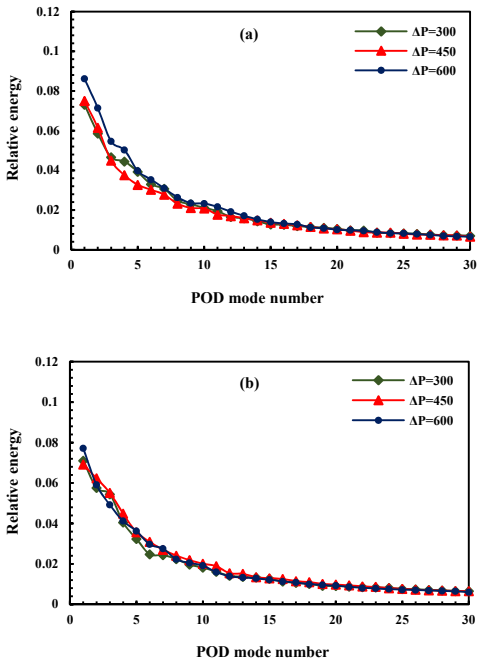

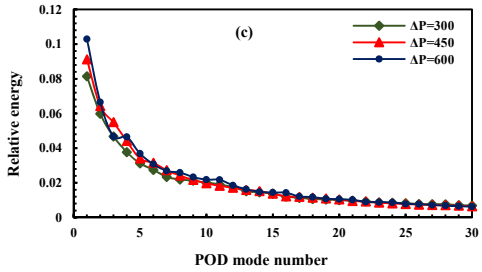

Fig. 7. Relative energy distribution for different pressure differences at (a) valve lift 2 mm, (b) valve lift 5 mm, (c) valve lift 9 mm.

4.5.2 Mode_1 and Mode_2 Structures at Different Valve Lifts

Proper Orthogonal Decomposition analysis were carried out on the experimental data obtained from PIV for all valve lift cases, however in this section, PIV data for valve-lift 9 and pressure differences ΔP=300, 450 and 600 mmH_2O are discussed here. Mode 1 and mode 2 structures are shown in Fig. 8. For ΔP=300 mmH_2O, the turbulent kinetic energy in mode 1 and mode 2 was 8% and 6% respectively.

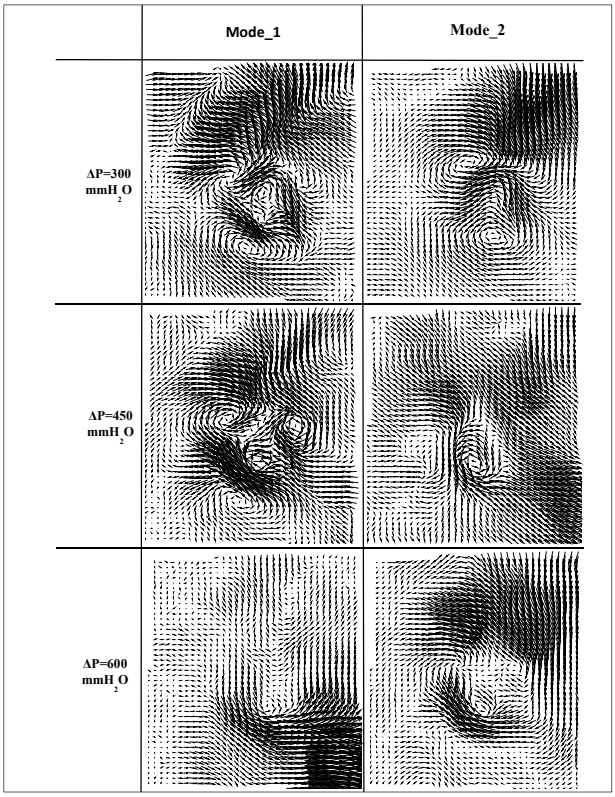

Fig. 8. Mode 1 and mode 2 spatial structures at valve lift 9 mm.

The spatial mode 1 identified low momentum fluid moving away from the bottom of the wall and a streak of high momentum fluid coming towards the bottom wall resulting in a clockwise rotating structure. Another clockwise rotating structure also formed due to interaction of streaks of high and low momentum fluid streams. On top of that, a large streak of strong vectors moved towards the cylinder head. Mode 2 partially exhibited the same pattern as of ensemble average of this case. This mode identified the same counter rotating structure but different in shape and position compared to the structure identified in the ensemble average. A clockwise rotating structure of the same size is also identified in the upper region. At the top right, a streak of velocity vectors moving down quite opposite to the vectors identified in the ensemble average were obvious. We conjectured that this change in direction might be due to its time-dependent coefficient. Since the total amount of kinetic energy in these two modes are low, no definite pattern similar to ensemble average was identified.

For ΔP=450 mmH_2O, the spatial mode 1 identified 4 vortical structures due to the interaction of streaks of high and low momentum fluid streams. The shape and size of these structures were almost same. Due to the small proportion of the energy contained in this mode, none of these structures or the flow patterns actually represented the total flow. Mode 2 identified one rotating structure in the middle and a large portion of streak of velocity vectors moving down towards the bottom wall. Therefore, a number of modes would be necessary for the representation of the actual flow.

For higher pressure difference ΔP=600 mmH_2O, the velocity would be higher eventually making the flow

more turbulent. The energy graph for this case showed that mode 1 contained 11.5% of the total kinetic energy. Mode 2 contained 6.6%, mode 3 contained 4.8%, and mode 4 contained 5% of the total kinetic energy. After mode 3, there was a slight increase in the energy contents for mode 4 hinting the cut off length. We conjectured that the first four modes might be sufficient in this case for the representation of the flow field. Mode 1 in this case identified some flow patterns similar to the ensemble average. At the bottom, a streak of velocity vectors was found to move towards the right and then up. In the upper section, there were small and random

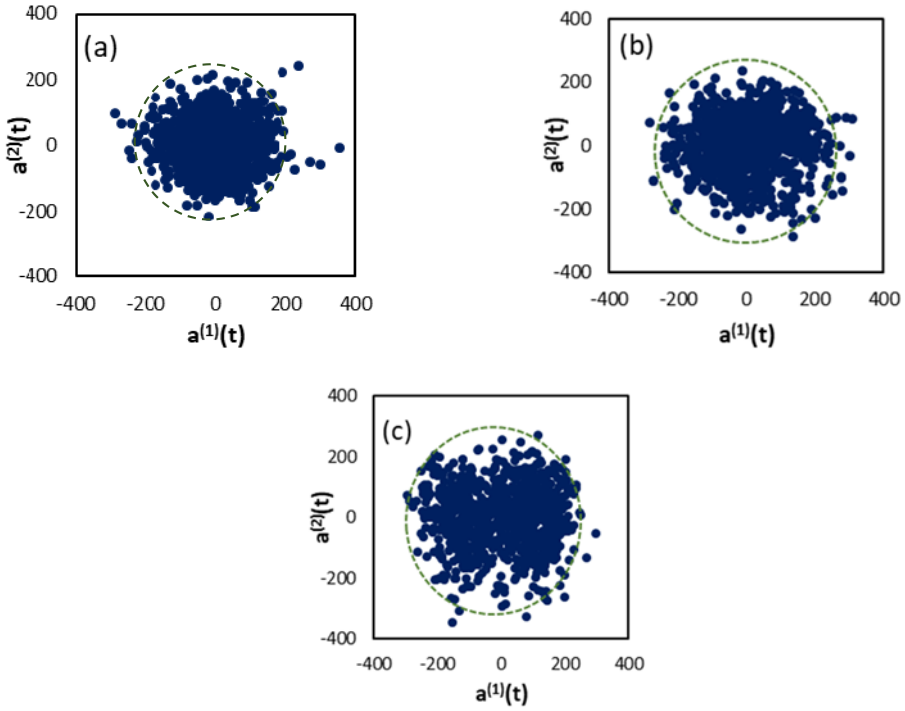

Fig. 9. POD coefficients for modes 1 and 2 at valve lift 9 (a) ΔP=300 mmH₂O, (b) ΔP=450 mmH₂O, (c) ΔP=600 mmH₂O.

velocity vectors in all directions. No dominant structure representing the flow was identified in this mode. Mode 2, though, identified a weak clockwise rotating structure in the middle but at the bottom there were weak velocity vectors giving no meaningful information about the flow. In the upper half, vectors moving down were captured might be when multiplied with the coefficient reverses its direction. Based on this POD analysis, it can be said that the POD identified small and weak structures in the modes due to the small proportion of the kinetic energy they contained. These modes might not be able to represent the flow all alone again due to small energy but sufficient number of modes would produce good representation of the flow. It is also believed that none of the dominant structure would be able to influence the flow and a linear combination of modes can highlight the missing flow features from the modes.

4.5.3 POD Coefficients

To illustrate the correlation of the coefficients of the first two POD modes and their relative frequency in each mode, the $a^{(1)}(t)$ versus $a^{(2)}(t)$ for all cases of valve lift 9 are plotted in Fig. 9. The data show that for ΔP=300 mmH₂O, $a^{(1)}(t)$ versus $a^{(2)}(t)$ appeared in a circular format indicating that the two modes are highly correlated as both the modes highlighted small scale eddies. This circular nature also highlighted the fact that both the spatial modes have the same frequency. The same pattern was observed for ΔP=450 and 600 mmH₂O cases as shown in Fig. 9.

5. CONCLUSIONS

The effect of pressure difference across the intake valves on the temporal and spatial structure of the flow in the cylinder of a 4-valve GDI engine under steady-state conditions was investigated experimentally using Stereo-PIV. Averaged velocity vector fields obtained in mid cylinder plane were analyzed in order to understand the in-cylinder flow behavior. Furthermore, POD was applied on the time resolved PIV data sets to extract the most energetic structures impeded in the flow.

The following conclusions were drawn:

- The effect of the pressure difference on the flow structure and tumble ratio was negligible compared to the effect of valve lift.
- The vortices formed preserved their shape for the same valve lift for different pressure differences. The only change was the vortex strength which increased with increasing the pressure difference.

- For valve lift 9mm, the average turbulent kinetic energy increased by 36.7 % when the pressure difference increased from 300 to 450 mmH_2O, and by 10.7 % when the pressure difference increased from 450 to 600 mmH_2O.
- The relative energy distribution corresponding to the first POD modes for all cases was quite small which gave an indication to the complexity of the flow. Moreover, there were no significant differences in the relative energy distribution since the flow structure had not changed with changing the pressure differences across the intake valves.
- A high number of POD modes is required to produce good representation of the flow due to the small energy content in the different POD modes.

ACKNOWLEDGEMENT

The current work was carried out in a collaboration between Universiti Teknologi PETRONAS (UTP) through the Centre for Automotive Research and Energy Management (CAREM) (PRGS/1/2017/TK07/UTP/01/1) and Ricardo UK.

REFERENCES

Adomeit, P., R. Weinowski, J. Ewald, A. Brunn, H. Kleeberg, D. Tomazic and M. Jakob (2010). *A new approach for optimization of mixture formation on gasoline DI engines* (2010-01-0591). SAE Technical Paper.

Bari, S. and I. Saad (2013). CFD modelling of the effect of guide vane swirl and tumble device to generate better in-cylinder air flow in a CI engine fuelled by biodiesel. *Computers and Fluids 84*, 262-269.

Bizon, K., G. Continillo, K. C. Leistner, E. Mancaruso and B. M. Vaglieco (2009). POD-based analysis of cycle-to-cycle variations in an optically accessible diesel engine. *Proceedings of the Combustion Institute 32*(2), 2809-2816.

Brusiani, F., S. Falfari and G. Cazzoli (2014). Tumble motion generation in small gasoline engines: A new methodological approach for the analysis of the influence of the intake duct geometrical parameters. *Energy Procedia 45*, 997-1006.

Buhl, S., F. Gleiss, M. Köhler, F. Hartmann, D. Messig, C. Brücker and C. Hasse (2017). A combined numerical and experimental study of the 3D tumble structure and piston boundary layer development during the intake stroke of a gasoline engine. *Flow, Turbulence and Combustion 98*(2), 579-600.

Chen, H., D. Hung, M. Xu and J. Zhong (2013). Analyzing the cycle-to-cycle variations of pulsing spray characteristics by means of the proper orthogonal decomposition. *Atomization and Sprays 23*(7).

Chen, H., D. L. Reuss and V. Sick (2011). Analysis of misfires in a direct injection engine using proper orthogonal decomposition. *Experiments in fluids 51*(4), 1139.

Clenci, A. C., V. Iorga-Simăn, M. Deligant, P. Podevin, G. Descombes and R. Niculescu (2014). A CFD (computational fluid dynamics) study on the effects of operating an engine with low intake valve lift at idle corresponding speed. *Energy 71*, 202-217.

El-Adawy, M., Heikal, M. R., A Aziz, A. R., Siddiqui, M. I., & Munir, S. (2017a). Characterization of the Inlet Port Flow under Steady-State Conditions Using PIV and POD. *Energies, 10*(12), 1950.

El-Adawy, M., Heikal, M. R., Aziz, A. R. A., Siddiqui, M. I., & Wahhab, H. A. A. (2017b). Experimental study on an IC engine in-cylinder flow using different steady-state flow benches. *Alexandria Engineering Journal*.

Fogleman, M., J. Lumley, D. Rempfer and D. Haworth (2004). Application of the proper orthogonal decomposition to datasets of internal combustion engine flows. *Journal of Turbulence 5*(23), 1-3.

Fraidl, G. K., W. F. Piock and M. Wirth (1996). *Gasoline direct injection: actual trends and future strategies for injection and combustion systems* (No. 960465). SAE Technical Paper.

Fu, J., G. Zhu, F. Zhou, J. Liu, Y. Xia and S. Wang (2016). Experimental investigation on the influences of exhaust gas recirculation coupling with intake tumble on gasoline engine economy and emission performance. *Energy Conversion and Management 127*, 424-436.

Graftieaux, L., M. Michard and N. Grosjean (2001). Combining PIV, POD and vortex identification algorithms for the study of unsteady turbulent swirling flows. *Measurement Science and technology 12*(9), 1422.

Khalighi, B. (1991). Study of the intake tumble motion by flow visualization and particle tracking velocimetry. *Experiments in Fluids*, *10*(4), 230-236.

Kim, M., S. Lee and W. Kim (2006). Tumble flow measurements using three different methods and its effects on fuel economy and emissions. *SAE Technical Paper* (2006-01), 3345.

Krishna, A. S., J. M. Mallikarjuna and D. Kumar (2016). Effect of engine parameters on in-cylinder flows in a two-stroke gasoline direct injection engine. *Applied Energy 176*, 282-294.

Krishna, B. M. and J. M. Mallikarjuna (2011). Effect of engine speed on in-cylinder tumble flows in a motored internal combustion engine—an experimental investigation using particle image velocimetry. *J. Appl. Fluid Mech 4*(1), 1-14.

Lee, K., C. Bae and K. Kang (2007). The effects of tumble and swirl flows on flame propagation in a four-valve SI engine. *Applied thermal*

engineering, *27*(11), 2122-2130.

Li, W., Y. Li, T. Wang, M. Jia, Z. Che and D. Liu (2017). Investigation of the Effect of the In-Cylinder Tumble Motion on Cycle-to-Cycle Variations in a Direct Injection Spark Ignition (DISI) Engine Using Large Eddy Simulation (LES). *Flow, Turbulence and Combustion 98*(2), 601-631.

Li, Y., H. Zhao, Z. Peng and N. Ladommatos (2001). *Analysis of tumble and swirl motions in a four-valve SI engine* (No. 2001-01-3555). SAE Technical Paper.

Liu, K., D. C. Haworth, X. Yang and V. Gopalakrishnan (2013). Large-eddy simulation of motored flow in a two-valve piston engine: POD analysis and cycle-to-cycle variations. *Flow, turbulence and combustion 91*(2), 373-403.

Lumley, J. L. (1967). The structure of inhomogeneous turbulent flows. *Atmospheric turbulence and radio wave propagation*.

Ortmann, R., S. Arndt, J. Raimann, R. Grzeszik and G. Wuerfel (2001). *Methods and analysis of fuel injection, mixture preparation and charge stratification in different direct injected SI engines* (No. 2001-01-0970). SAE Technical Paper.

Preussner, C., C. Döring, S. Fehler and S. Kampmann (1998). *GDI: interaction between mixture preparation, combustion system and injector performance* (No. 980498). SAE Technical Paper.

Reuss, D. L. (2000). *Cyclic variability of large-scale turbulent structures in directed and undirected IC engine flows* (No. 2000-01-0246). SAE Technical Paper.

Ricardo, M. B., P. Apostolos and M. Yang (2011). Overview of boosting options for future downsized engines. *Science China Technological Sciences 54*(2), 318-331.

Sick, V., H. Chen, P. S. Abraham, D. L. Reuss, X. Yang, V. Gopalakrishnan and T. W. Kuo (2012). Proper-orthogonal decomposition analysis for engine research. In *9th Congress, Gasoline Direct Injection Engines, Essen, Germany* (1-12).

Sirovich, L. (1987). Turbulence and the dynamics of coherent structures. I. Coherent structures. *Quarterly of applied mathematics 45*(3), 561-571.

Smith, J. D. and V. Sick (2006). *A multi-variable high-speed imaging study of ignition instabilities in a spray-guided direct-injected spark-ignition engine* (2006-01-1264). SAE Technical Paper.

Wang, T., W. Li, M. Jia, D. Liu, W. Qin and X. Zhang (2015). Large-eddy simulation of in-cylinder flow in a DISI engine with charge motion control valve: Proper orthogonal decomposition analysis and cyclic variation. *Applied Thermal Engineering 75*, 561-574.

Yang, X., T. W. Kuo , O. Guralp, R. O. Grover and P. Najt (2017). In-Cylinder Flow Correlations between Steady Flow Bench and Motored Engine Using Computational Fluid Dynamics. *Journal of Engineering for Gas Turbines and Power 139*(7), 072802.

Zhang, X., T. Wang, M. Jia, W. Li, L. Cui and X. Zhang (2015). The Interactions of In-Cylinder Flow and Fuel Spray in a Gasoline Direct Injection Engine with Variable Tumble. *Journal of Engineering for Gas Turbines and Power 137*(7), 071507.

Zhang, Z., H. Zhang, T. Wang and M. Jia (2014). Effects of tumble combined with EGR (exhaust gas recirculation) on the combustion and emissions in a spark ignition engine at part loads. *Energy 65*, 18-24.

Zhao, F., M. C. Lai and D. L. Harrington (1999). Automotive spark-ignited direct-injection gasoline engines. *Progress in energy and combustion science*, *25*(5), 437-562.